A&A 484, 679–691 (2008)
DOI: 10.1051/0004-6361:20078121

Astronomy & Astrophysics

Formation of [α/Fe] radial gradients in the stars of elliptical galaxies

A. Pipino[1,3], A. D'Ercole[2], and F. Matteucci[3]

[1] Astrophysics, University of Oxford, Denys Wilkinson Building, Keble Road, Oxford OX1 3RH, UK
e-mail: axp@astro.ox.ac.uk
[2] INAF - Osservatorio Astronomico di Bologna, via Ranzani 1, 40127 Bologna, Italy
[3] Dipartimento di Astronomia, Università di Trieste, via G.B. Tiepolo 11, 34100 Trieste, Italy

Received 20 June 2007 / Accepted 1 April 2008

ABSTRACT

Aims. We aim: i) to test and improve our previous models of an outside-in formation for the majority of ellipticals in the context of the SN-driven wind scenario, by means of a careful study of gas inflows/outflows; ii) to explain the observed slopes, either positive or negative, in the radial gradient of the mean stellar [α/Fe], and their apparent lack of correlation with all other observables.
Methods. We present a new class of hydrodynamical simulations for the formation of single elliptical galaxies in which we implement detailed prescriptions for the chemical evolution of H, He, O and Fe.
Results. We find that all the models that predict chemical properties (such as the central mass-weighted abundance ratios, the colours or the [⟨Fe/H⟩] gradient) that lie within the observed ranges for a typical elliptical, also exhibit a variety of gradients in the [⟨α/Fe⟩] ratio, in agreement with the observations (namely positive, null or negative). All these models undergo an outside-in formation, in the sense that star formation stops earlier in the outermost than in the innermost regions, due to the onset of a galactic wind. We find that the predicted variety of gradients in the [⟨α/Fe⟩] ratio can be explained by physical processes generally not taken into account in simple chemical evolution models, such as radial flows coupled with different initial conditions for the galactic proto-cloud. The typical [⟨Z/H⟩] gradients predicted by our models have a slope of –0.3 dex per decade variation in radius, consistent with the mean values of several observational samples. However, we also find a quite extreme model in which this slope is –0.5 dex per decade, thus explaining some recent data on gradients in ellipticals.
Conclusions. We conclude that the history of star formation is fundamental for the creation of abundance gradients in ellipticals but that radial flows with different velocity in conjunction with the duration and efficiency of star formation in different galactic regions are responsible for the gradients in the [⟨α/Fe⟩] ratios.

Key words. galaxies: aboundances – galaxies: elliptical and lenticular, cD – galaxies: evolution – galaxies: formation

1. Introduction

In this paper we exploit the radial variations in the chemical properties of the Composite Stellar Populations (CSPs) inhabiting elliptical galaxies in order to gain new insights into the mechanism of galaxy formation. Theoretical investigations show that these properties strongly vary as a function of either the duration or the intensity of the star formation (SF), as well as of the infall history at each radius. A useful tool to understand the complex issue of galaxy formation is the study of the radial gradients in either the mean abundance ratios or in the mean metallicity in the stars. There is general consensus that the observed increase of line-strength indices such as the Mg_2 and the ⟨Fe⟩ (e.g. Carollo et al. 1993; Davies et al. 1993; Trager et al. 2000a) and the reddening of the colours (e.g. Peletier et al. 1990), toward the centre of elliptical galaxies should be interpreted as an increase in the mean metallicity of the underlying stellar populations. In particular, the existence of possible trends of the gradient slopes with galactic mass not only could favour a specific galaxy formation scenario, but also might tell us about the degree of uniformity of this process. Davies et al. (1993) did not find any correlation linking the gradients to the mass or the Mg_2 of the galaxies, whereas Carollo et al. (1993) claimed a bimodal trend with mass, in which the Mg_2 gradient grows with mass below a certain galactic mass ($\sim 10^{11}$ $M_\odot$) and becomes flatter in more massive ellipticals. On the other hand, Gonzalez & Gorgas (1996) found that the gradient correlates better with the central value of Mg_2 than with any other global parameter. Kobayashi & Arimoto (1999) analysed a compilation of data in the literature, finding that the metallicity gradients do not correlate with any physical property of the galaxies, including central indices and velocity dispersion, as well as mass and B magnitude. Ogando et al. (2005) claimed that the relation originally found by Carollo et al. (1993), for low mass ellipticals might be extended to very massive spheroids (see also Forbes et al. 2005).

From a theoretical point of view dissipative collapse models (Larson 1974; Carlberg 1984) predicted quite steep gradients that correlate with galactic mass. Mergers, on the other hand, are expected to dilute the gradients (Kobayashi 2004). In the framework of chemical evolution models, Martinelli et al. (1998) suggested that gradients can arise as a consequence of a more prolonged SF, and thus stronger chemical enrichment, in the inner zones. In the galactic core the potential well is deeper and the supernovae (SN) driven wind develops later relative to the most external regions (see also Carollo et al. 1993). Similar conclusions were found by Pipino & Matteucci (2004, PM04), with a more sophisticated model which also takes into accont the initial infall of gas plus a galactic wind triggered by SN activity. The PM04 model predicts a logarithmic slope for indices such

as Mg_2 which is very close to typical observed gradients, and, on average, seems to be independent of the mass of the galaxies.

Gradients in abundance ratios such as the [α/Fe] ratio are in principle very important, since we could use them as a measure for the duration of the SF process in that region (see Matteucci & Greggio 1986; Matteucci 1994). However, we will show that the estimate of the *relative* duration of the star formation process between two different galactic regions with similar mean [α/Fe] ratios in their stars ([⟨α/Fe⟩], hereafter) is also affected by either the *local* SF efficiency or by (differential) metal-enhanced gas flows. This is one of the main novelties of our approach with respect to our previous work. A prediction made by the PM04 best model was that the galaxy should form outside-in with an increase in the [⟨α/Fe⟩] ratio as a function of the radius. To date, only a handful of observational works inferred the gradients in the [⟨α/Fe⟩] ratios from the indices such as Mg_2 and ⟨Fe⟩ (Melhert et al. 2003; Annibali et al. 2007; Sanchez-Blazquez et al. 2007). These papers show that the slope in the [⟨α/Fe⟩] gradient can be either negative or positive, with a mean value close to zero, and that it does not correlate with galactic properties. In other words, they suggest that there is not a preferred mechanism for the formation of single galaxies, such as either an outside-in or an inside-out mechanism. A drawback of these studies is that their samples are relatively small and the variations in the indices were often evaluated either well inside one effective radius or by neglecting the galactic core, thus rendering the compilations of the slopes not homogeneous. On the other hand, a few recently observed single galaxies (NGC 4697, Mendez et al. 2005; NGC 821, Proctor et al. 2005, even though in the latter the authors use an empirical conversion in order to obtain [O/Fe]), seem to support PM04's predictions, as shown by Pipino et al. (2006, PMC06). PMC06 also stressed the fact the ellipticals are made of composite stellar populations with properties changing with radius; therefore, it cannot be taken for granted that the abundance pattern used to build theoretical single stellar populations (SSPs) and to infer abundance ratios from the line indices really reflect the true chemical composition of the stars (see also Serra & Trager 2006).

Finally, a limitation of the chemical evolution models is that gas flows cannot be treated with the same detail of a hydrodynamical model. This may affect not only the infall history or the development of the galactic wind, but also hampers an estimate of the role of possible internal flows on the build-up of the gradients.

The aim of this paper is, therefore, manyfold:

i) to test the PM04 prediction of an outside-in formation for the majority of ellipticals in the context of the SN-driven wind scenario by means of a careful study of gas inflows/outflows;
ii) to improve the PM04 formulation by a detailed treatment of gas dynamics;
iii) to show how the observed variety of slopes in the [⟨α/Fe⟩] gradients in stars might be related to the different initial conditions and reconciled within a quasi-monolithic formation scenario.

In this sense we complete and supersede the work of Kobayashi (2004), who, with SPH models, studied only the metallicity gradients and found that nearly half of ellipticals have a pure monolithic origin, while the other half had undergone mergers during their life. In order to do that, we couple a simplified chemical evolution scheme with the hydrodynamical code (Bedogni & D'Ercole 1986; Ciotti et al. 1991) presented in Sect. 2. Our model results will be discussed in Sects. 3, 4 and 5; we summarise our main conclusions in Sect. 6.

2. The model

2.1. Hydrodynamics

We adopted a one-dimensional hydrodynamical model that follows the time evolution of the density of mass (ρ), momentum (m) and internal energy (ε) of a galaxy, under the assumption of spherical symmetry. In order to solve the equation of hydrodynamics with a source term we made use of the code presented in Ciotti et al. (1991), which is an improved version of the Bedogni & D'Ercole (1986) Eulerian, second-order, upwind integration scheme (see their Appendix), to which we refer the reader for a thorough description of both the set of equations and their solutions. Here we report the gas-dynamical equations:

$$\frac{\partial \rho}{\partial t} + \nabla \cdot (\rho u) = \alpha \rho_* - \Psi, \tag{1}$$

$$\frac{\partial \varrho^i}{\partial t} + \nabla \cdot (\varrho^i u) = \alpha^i \rho_* - \Psi \varrho^i / \rho, \tag{2}$$

$$\frac{\partial m}{\partial t} + \nabla \cdot (m u) = \rho g - (\gamma - 1)\nabla \varepsilon - \Psi u, \tag{3}$$

$$\frac{\partial \varepsilon}{\partial t} + \nabla \cdot (\varepsilon u) = -(\gamma - 1)\varepsilon \nabla \cdot u - L + \alpha \rho_* \left(\epsilon_0 + \frac{1}{2}u^2\right) - \Psi \varepsilon / \rho. \tag{4}$$

The parameter $\gamma = 5/3$ is the ratio of the specific heats, g and u are the gravitational acceleration and the fluid velocity, respectively. The source terms on the rhs of Eqs. (1)–(4) describe the injection of total mass and energy in the gas due to the mass return and energy input from the stars. $\alpha(t) = \alpha_*(t) + \alpha_{\rm SNII}(t) + \alpha_{\rm SNIa}(t)$ is the sum of the specific mass return rates from low-mass stars and SNe of both type II and Ia, respectively. ϵ_0 is the injection energy per unit mass due to SN explosions (see Sect. 2.2). Ψ is the astration term due to SF. $L = n_{\rm e} n_{\rm p} \Lambda(T, Z)$ is the cooling rate per unit volume, where for the cooling law, $\Lambda(T, Z)$, we adopt the Sutherland & Dopita (1993) curves. This treatment allows us to implement a self-consistent dependence of the cooling curve on the metallicity (Z) in the present code. We do not allow the gas temperature to drop below 10^4 K. This assumption does not affect the conclusions.

ϱ^i represents the mass density of the ith element, and α^i the specific mass return rate for the same element, with $\sum_{i=1}^{N} \alpha^i = \alpha$. Equation (2) represents a subsystem of four equations that follow the hydrodynamical evolution of four different ejected elements (namely H, He, O and Fe). We divide the grid in 550 zones 10 pc wide in the innermost regions, and then slightly increasing with a size ratio between adjacent zones equal to 1.03. This choice allows us to properly sample the galaxies without wasting computational resources on the fraction of the simulated box at distances comparable to the galactic tidal radius (see Sect. 2.3 for its value). At the same time, however, the size of the simulated box is roughly a factor of 10 larger than the stellar tidal radius. This is necessary to avoid possible perturbations at the boundary affecting the galaxy and because we want to have a surrounding medium that acts as a gas reservoir for the models in which we start from an initial flat gas density distribution (see Sect. 2 for the model definition). We adopted a reflecting boundary condition in the center of the grid and allowed for an outflow condition in the outermost point.

At every point of the mesh we allow the SF to occur at the following rate:

$$\Psi = \nu \rho = \frac{\epsilon_{\rm SF}}{\max(t_{\rm cool}, t_{\rm ff})} \rho \tag{5}$$

where $t_{\rm cool}$ and $t_{\rm ff}$ are the *local* cooling and free-fall timescales, respectively, and $\epsilon_{\rm SF}$ is a suitable *SF parameter* that contains all the uncertainties on the timescales of the SF process that cannot be taken into account in the present modelling and its value is given a priori. In particular, we stress that the adopted parametrization of the SF process might appear simplistic, although it is a rather standard assumption in many galaxy formation simulations where the sub-grid physics cannot be properly modelled. A more detailed representation should at least discriminate between a cold molecular gas phase which is actually feeding the SF process, and the hot surrounding medium where the ejecta from SN are deposited. On the other hand, Eq. (5) does not imply that SF is occurring in the hot gas phase; in fact, we assume that a suitable fraction proportional to the average density in the gridpoint forms stars once it has cooled down[1].

ν gives the speed of the SF process; the *final efficiency*, namely the fraction of gas that eventually turned into stars, is an output of the model.

We assume that the stars do not move from the gridpoint at which they have been formed. We are aware that this can be a limitation of the model, but we prefer this solution to moving the stars in order to match some pre-defined luminosity profile (as done in, e.g., Friaca & Terlevich 1998), because this might artificially affect the resulting metallicity gradients. Moreover, we expect that the stars will spend most of their time close to their apocentre. In order to ensure that we match the observed mass-to-light ratio for the given potential well, we stop the SF in a given grid-point only if the mass density of low-mass stars created at that radius exceeds a given threshold profile. The adopted profile is a King distribution, with a core radius of 370 pc and a central stellar mass density of 6×10^{-21}g cm^{-3}. Integrating over the whole galactic volume, the above mentioned limiting profile yields a total stellar mass of $\sim 3 \times 10^{11}$ $M_{\odot}$. In the next section we will show that this assumption does not invalidate our simulated galaxies, because the occurrence of a galactic wind, which halts the SF process, coincides with or occurs even earlier than the time at which such a threshold profile is attained.

At the beginning the gas is subject only to the Dark Matter (DM) halo gravity and to its own self-gravity; once SF begins, the gravitational potential due to the stellar component is self-consistently evaluated.

The DM potential has been evaluated by assuming a distribution inversely proportional to the square of the radius at large distances (see Silich & Tenorio-Tagle 1998). We classify each model according to the size of the DM halo (see next section). The adopted core radii for the DM distribution are reported in Table 1.

Table 1. Input parameters.

Model	$R_{\rm core,DM}$ (kpc)	$R_{\rm core,gas}$ (kpc)	$\rho_{\rm core,gas}$ (10^{-25}g cm^{-3})	$\epsilon_{\rm SF}$	T (K)	$\epsilon_{\rm SN}$
Ma1	1.5	0.4	0.6	1	10^6	0.1
Ma2	1.5	0.4	0.6	10	10^4	0.1
Ma3	1.5	0.4	0.6	2	10^4	0.1
MaSN	1.5	0.4	0.6	1	10^6	1.0
Mb1	1.5	–	0.06	1	10^7	0.1
Mb2	1.5	–	0.2	1	10^5	0.1
Mb3	1.5	–	0.06	10	10^6	0.1
Mb4	1.5	–	0.6	1	10^6	0.1
Mb5	1.5	0.4	0.6	2	10^4	0.1
La	4.5	1.0	0.6	10	10^7	0.1
Lb	4.5	–	0.6	10	10^6	0.1

2.2. Chemical evolution

We follow the chemical evolution of only four elements, H, He, O and Fe. This set of elements is good enough to characterize our simulated elliptical galaxy from the chemical evolution point of view. As shown by the time-delay model (Matteucci & Greggio 1986, see also PMC06), the [α/Fe] ratio is a powerful estimator of the duration of SF. Moreover, both the predicted [Fe/H]-mass and [Z/H]-mass relationships in the stars can be tested against the observed colour-magnitude relations (hereafter CMRs; e.g. Bower et al. 1992), and mass-metallicity relation (hereafter MMR; e.g. Carollo et al. 1993). O is the major contributor to the total metallicity, therefore its abundance is a good tracer of the metal abundance Z. However, we always refer to Z as the sum of the O and Fe mass abundances. On the other hand, the Fe abundance is probably the most commonly used probe of the metal content in stars, therefore it enables a quick comparison between our model predictions and the existing literature. In the past literature the majority of the works used Mg as a proxy for the α elements, as can be easily observed in absorption in the optical bands giving rise to the well known Mg_2 and Mg_b Lick indices. However, the state-of-the-art SSPs libraries (Thomas et al. 2003; Lee & Worthey 2005) are computed as functions of the *total* α-enhancement and of the total metallicity. Moreover the latest observational results (Mehlert et al. 2003; Annibali et al. 2007; Sanchez-Blazquez et al. 2007) have been translated into theoretical ones by means of these SSPs; therefore the above authors provide us with radial gradients in [α/Fe], instead of [Mg/Fe]. This is why in this paper we focus on the theoretical evolution of the α elements, and the O is by far the most important. We will also present our predictions in the form of indices and show that we obtain reasonable values in agreement with observations. We will compare our results to recent observational data that have been transformed into abundance ratios by means of SSPs computed assuming a global α-enhancement. Finally, on the basis of nucleosynthesis calculations, we expect O and Mg to evolve in parallel. This means that the [O/Fe] = [Mg/Fe] + const. equation should hold (in the gas) during galactic evolution (see e.g. Fig. 1 of PM04); therefore the predicted slope of the [α/Fe] gradient in the stars should not change if we adopt either O or Mg as a proxy for the αs. There might be only an offset in the zero point of, at most, 0.1–0.2 dex which is within both the observed scatter and the uncertainties of the *calibration* used to transform Lick indices into abundance ratios.

The nucleosynthetic products enter the mass conservation equations via several source terms, according to their stellar origin. A Salpeter (1955) initial mass function (IMF) constant in time in the range 0.1–50 $M_{\odot}$ is assumed, since PM04 and PMC06 showed that the majority of the photochemical properties of an elliptical galaxy can be reproduced with this choice for the IMF. We adopted the yields from (Iwamoto et al. 1999, and references therein) for both SNIa and SNII. The SNIa rate for a SSP formed at a given radius is calculated assuming the single degenerate scenario and the Matteucci & Recchi (2001) delay time distribution (DTD). The convolution of this DTD with Ψ over the galactic volume gives the total SNIa rate, according to the following equation (see Greggio 2005):

$$r_{\rm Ia}(t) = k_{\alpha} \int_{\tau_i}^{\min(t,\tau_x)} A(t-\tau)\Psi(t-\tau)DTD(\tau)\mathrm{d}\tau \qquad (6)$$

[1] Note also that $\Psi \to 0$ if $t_{\rm cool} \to \infty$, namely if the gas is cooling on a very long timescale.

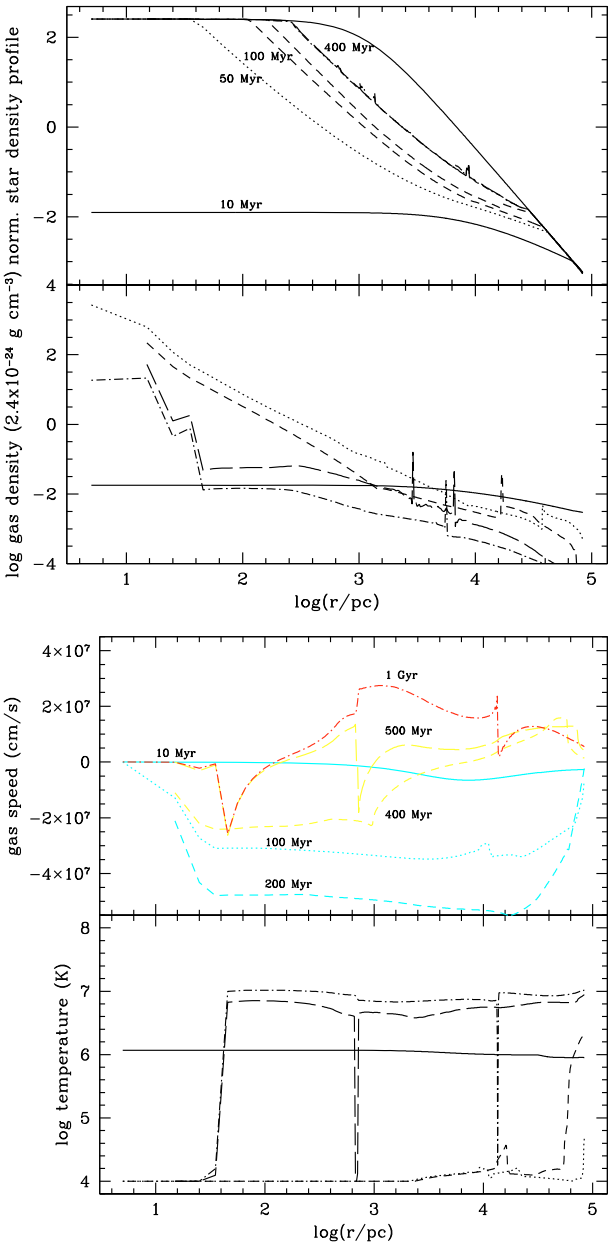

Fig. 1. *Upper panels*: the stellar mass- (*top*) and gas density (*bottom*) profiles predicted by model La at different times: 10 Myr (solid), 50 Myr (dotted), 100 Myr and 200 Myr (dashed), 400 Myr (dotted-dashed). The model predictions at 1 Gyr coincide with the ones at 400 Myr. The thick solid line without time labels represents a King profile (see text). *Lower panels*: the gas velocity (*top*) and temperature (*bottom*) profiles predicted by model La at different times: 10 Myr (solid), 100 Myr (dotted), 200 Myr (thick-dashed), 400 Myr and 500 Myr (thin-dashed), 1 Gyr (dotted-dashed).

where $A(t-\tau)$ is the fraction of binary systems that give rise to type Ia SNe. Here we will assume it constant (see Matteucci et al. 2006, for a more detailed discussion). The time τ is the delay time defined in the range (τ_i, τ_x) so that:

$$\int_{\tau_i}^{\tau_x} DTD(\tau)\mathrm{d}\tau = 1 \tag{7}$$

where τ_i is the minimum delay time for the occurrence of type Ia SNe, in other words the time at which the first SNe Ia start occurring. We assume for this new formulation of the SNIa rate that τ_i is the lifetime of a 8 $M_\odot$ star, while for τ_x, which is the maximum delay time, we assume the lifetime of 0.8 $M_\odot$. The DTD gives the likelihood that at a given time a binary system will explode as a SNIa. Finally, k_α is the number of stars per unit mass in a stellar generation and contains the IMF.

According to the adopted model progenitor and nucleosynthetic yields, each SNIa explosion releases $E_0 = \epsilon_{\rm SN}\, 10^{51}$ erg of energy and 1.4 $M_\odot$ of mass (out of which 0.1 $M_\odot$ of O and 0.7 $M_\odot$ of Fe, respectively). For simplicity, we assume that the progenitor of SNII is a typical *average* (in the range 10–50 $M_\odot$) massive star of 18.6 $M_\odot$, which pollutes the ISM with ~17 $M_\odot$ of ejecta during the explosion (of which 1.8 $M_\odot$ of O and 0.08 $M_\odot$ of Fe). We recall that single low- and intermediate-mass stars do not contribute to the production of either Fe or O. We neglect the fact that they may lock some heavy elements present in the gas out of which they formed, and restore them on very long timescales; therefore single low- and intermediate-mass stars are only responsible for the ejection of H and He. Such a simplified scheme has been tested with our chemical evolution code (PM04, their model IIb); it leads to relative changes of less than the 10% in the predicted abundance ratios with respect to the ones predicted with the full solution of the chemical evolution equations.

These quantities, as well as the evolution of single low and intermediate mass stars, were evaluated by adopting the stellar lifetimes given by Padovani & Matteucci (1993). The solar abundances are taken from Asplund et al. (2005).

In order to study the mean properties of the stellar component in ellipticals, we need average quantities related to the mean abundance pattern of the stars, which, in turn, can allow a comparison with the observed integrated spectra. To this scope, we recall that, at a given radius, both real and model galaxies are made of CSP, namely a mixture of several SSP, differing in age and chemical composition according to the galactic chemical enrichment history, weighted with the SF rate. On the other hand, the line-strength indices are usually tabulated only for SSPs as functions of their age, metallicity and (possibly) α-enhancement.

In particular we make use of the mass-weighted mean stellar metallicity as defined by Pagel & Patchett (1975, see also Matteucci 1994):

$$\langle Z\rangle = \frac{1}{S_f}\int_0^{S_f} Z(S)\,\mathrm{d}S, \tag{8}$$

where S_f is the total mass of stars ever born contributing to the light at the present time and Z is the metal abundance (by mass) in the gas out of which an amout of stars S formed. In practice, we make use of the stellar mass distribution as a function of Z in order to derive the mean metallicity in stars.

One can further adapt Eq. (8) in order to calculate the mean O/Fe ratio in stars. In this case, however, we make use of the stellar mass distribution as a function of O/Fe. Therefore we obtain:

$$\langle \mathrm{O/Fe}\rangle = \frac{1}{S_f}\int_0^{S_f} (\mathrm{O/Fe})(S)\mathrm{d}S, \tag{9}$$

where now $(\mathrm{O/Fe})(S)$ is the abundance ratio characterising the gas out of which a mass dS of stars formed. This procedure will be repeated at each grid-point unless specified otherwise.

Then, we derive $[\langle \mathrm{O/Fe}\rangle] = \log(\langle \mathrm{O/Fe}\rangle) - \log(\mathrm{O/Fe})_\odot$, taking the logarithm after the average evaluation (see Gibson 1996). Similar equations hold for $[\langle \mathrm{Fe/H}\rangle]$ and the global metallicity $[\langle Z/H\rangle]$.

Another way to estimate the average composition of a CSP which is closer to the actual observational value is to use the V-luminosity weighted abundances (which will be denoted as $\langle O/Fe\rangle_V$). Following Arimoto & Yoshii (1987), we have:

$$\langle O/Fe\rangle_V = \sum_{k,l} n_{k,l}(O/Fe)_l L_{V,k} / \sum_{k,l} n_{k,l} L_{V,k}, \quad (10)$$

where $n_{k,l}$ is the number of stars binned in the interval centered around $(O/Fe)_l$ with V-band luminosity $L_{V,k}$. Generally the mass averaged [Fe/H] and [Z/H] are slightly larger than the luminosity averaged ones, except for large galaxies (see Yoshii & Arimoto 1987; Matteucci et al. 1998). However there might be differences between the two methods at large radii, as far as [Fe/H] and [Z/H] are concerned. In fact, the preliminary analysis of PMC06 showed that both distributions may be broad and asymmetric and their mean values can provide a poor estimate of the metallicity in complex systems with a chemical evolution history quite extended in time. On the other hand, PMC06 found the [Mg/Fe] distribution to be much more symmetric and narrow than the [Z/H] distribution. Therefore, we expect that $[\langle O/Fe\rangle] \simeq [\langle O/Fe\rangle_V]$ at any radius and hence, we present mass-weighted values that are more representative of the physical processes acting inside the galaxy. After PMC06, we will present our results in terms of $[\langle Fe/H\rangle_V]$ and $[\langle Z/H\rangle_V]$, because the luminosity-weighted mean is much closer to the actual observations and might differ from the mass-average, unless otherwise stated.

In order to convert the predicted abundances for a CSP into indices (especially in the case of short burst of SF), it is typically assumed that a SSP with a *mean* metallicity is representative of the whole galaxy. In other words, we use the predicted abundance ratios in stars for our CSPs to derive the line-strength indices for our model galaxies by selecting a SSP with the same values for $[\langle O/Fe\rangle]$, $[\langle Fe/H\rangle_V]$ and $[\langle H\rangle_V]$ from the compilation of Thomas et al. (2003, TMB03 hereafter).

2.3. Model description

The present work is aimed at understanding the origin of the radial gradients in the stars by means of models that have photochemical properties as well as radii comparable with those of typical massive ellipticals. Moreover, we would like to understand what causes the $[\langle\alpha/Fe\rangle]$ gradient slope to span the range of values ∼–0.2–+0.2 dex per decade in radius. In order to do that, we will vary the initial conditions by adopting reasonable hypotheses for the gas properties. A first classification of our set of models can be made according to their initial conditions (DM halo mass and available reservoir of gas):

- Model M: a 2.2×10^{12} $M_\odot$ DM halo and $\sim 2 \times 10^{11}$ $M_\odot$ of gas;
- Model L: a 5.7×10^{12} $M_\odot$ DM halo and $\sim 6.4 \times 10^{11}$ $M_\odot$ of gas.

These quantitites have been choosen to ensure a final ratio between the mass of baryons in stars and the mass of the DM halo of around 0.1. Models by Matteucci (1992), and PM04 require such a ratio for ellipticals in order to develop a galactic wind. A more refined treatment of the link between baryons and DM is beyond the scope of this work, and a more robust study of the gradient creation in a cosmological framework will be the topic of a forthcoming paper. The exact initial gas mass depends on the initial conditions and it is clear that gas can be accreted by the external environment. In particular, for each model we considered the following cases for the initial gas distribution:

a) Isothermal density profile. In this case, the gas is assumed to start from an isothermal configuration of equilibrium within the galactic (i.e. considering both DM and gas) potential well. The actual initial temperature is lower than the virial temperature, in order to induce the gas to collapse. These initial conditions might not be justified by the current Cold DM paradigm for the formation of structures. However, we consider them to be very useful because they give the closest approximation of the typical initial conditions adopted by the chemical evolution models to which we will compare our results. This is an extreme case in which we let all the gas be accreted before the SF starts.
b) Constant density profile. In this case the gas has an initial value for the mass density that is constant with radius in the whole computational box (cf. Sect. 2.1). The DM and, afterwards, the gas and stellar gravity will then create the conditions for a radial inflow. This case might be more realistic than the former one, in the sense that the DM potential will "perturb" the gas which is uniformly distributed at the beginning of the simulation. At variance with the previous model, in this case we let the SF process start at the same time as the gas accretion.

Table 1 summarises the main properties of each model in this paper, namely the core radius for both the DM and the gas profile, the SF parameter ϵ_{SF}, the initial temperature and the SN efficiency ϵ_{SN}.

Concerning the class of models labelled *a*, we mainly vary the gas temperature and the parameter of star formation. We do not vary the gas mass (via the core gas density and radius) because we need that precise amount of gas in order to ensure that: i) enough stars can be created; ii) at the same time there is not too much gas left (as present-day ellipticals are almost without gas). Also, the assumed profile guarantees that most of the gas is already within the final effective radius of the galaxy in a way that mimicks the assumptions made in PM04 and PMC06.

For the class of models labelled *b*, instead, the initial gas density (as reported in Table 1 under the column $\rho_{core,gas}$) can be a crucial parameter, as well as the gas temperature and ϵ_{SF}. Here the values for $\rho(r, t = 0) = \rho_{core,gas}$ is chosen in order to have the initial gas content in the whole grid not higher than the typical baryon fraction in a high density environment (i.e. 1/5–1/10 as in a galaxy cluster, e.g. McCarthy et al. 2007). In each case, the gas temperature ranges from 10^{4-5} K (cold-warm gas) to 10^{6-7} K (virialised haloes). We limit both the DM and the stellar profile to their tidal radii, chosen to be 66 kpc (both of them) in case M as well as 200 kpc and 100 kpc, respectively, in case L. These values are consistent with the radii of the X-ray haloes surrounding ellipticals of the same mass.

3. Results: a general overview

The main results of our models are presented in Table 2, where the final (i.e. after SF stops) values for the stellar core and effective radii, the time for the onset of the galactic wind in the central region (t_{gw}), the abundance ratios in the galactic center and the gradients in $[\langle O/Fe\rangle]$ and $[\langle Fe/H\rangle_V]$, are reported. In particular, we choose $R_{eff,*}$ as the radius that contains 1/2 of the stellar mass of the galaxy and, therefore, is directly comparable with the observed effective radius, whereas $R_{core,*}$ is the radius encompassing 1/10 of the galactic stellar mass. In most

Table 2. Model results.

Model	M_* (10^{10} $M_\odot$)	$R_{\rm core,*}$ (kpc)	$R_{\rm eff,*}$ (kpc)	$t_{\rm gw,core}$ (Myr)	$[\langle {\rm O/Fe}\rangle_{*,\rm core}]$	$[\langle {\rm Fe/H}\rangle_{*,\rm core}]$	$\Delta_{\rm O/Fe}$	$\Delta_{\rm Fe/H}$
Ma1	6.0	0.3	12	1100	0.29	0.13	0.02	–0.13
Ma2	25.	0.4	7.7	800	0.22	0.35	–0.21	–0.16
Ma3	25.	0.4	8.3	800	0.35	0.57	–0.17	–0.03
MaSN	2.0	6.6	31	200	0.55	–0.51	–0.14	+0.27
Mb1	6.0	0.4	17	700	0.14	0.22	0.09	–0.31
Mb2	3.0	0.2	8.7	300	0.33	–0.02	0.	–0.18
Mb3	21	0.4	8.8	440	0.17	0.37	–0.08	–0.29
Mb4	26	0.4	5.4	200	0.42	–0.40	–0.08	–0.20
Mb5	25.	14.8	33.6	1400	0.36	0.17	–0.14	–1.40
La	26	3.4	29	400	0.14	0.70	0.19	–0.50
Lb	29	2	21	400	0.12	0.57	0.32	–0.50

Values predicted after the SF has finished.

cases, this radius will correspond to ~0.05–0.2 $R_{\rm eff,*}$, which is the typical size of the aperture used in many observational works to measure the abundances in the innermost part of ellipticals. We did not fix $R_{\rm core,*} = 0.1R_{\rm eff,*}$ a priori, in order to have a more meaningful quantity, which may carry information on the actual simulated stellar profile. Finally, we use the following notation for the metallicity gradients in stars $\Delta_{\rm O/Fe} = ([\langle {\rm O/Fe}\rangle]_{\rm core} - [\langle {\rm O/Fe}\rangle]_{\rm eff})/\log(R_{\rm core,*}/R_{\rm eff,*})$; a similar expression applies for both the $[\langle {\rm Fe/H}\rangle_V]$ and the $[\langle Z/H\rangle_V]$ ratios.

The slope is calculated by a linear regression between the core and the half-mass radius, unless otherwise stated. Clearly, deviations from linearity can affect the slope at intermediate radii. Before discussing in detail the galactic formation mechanism of our models, we must check whether they resemble typical ellipticals for a given mass. First, we have to ensure that the MMR is satisfied. The majority of our model galaxies exhibit a central mean value of $[\langle {\rm Fe/H}\rangle_V]$ within the range inferred from integrated spectra, namely from –0.8 to 0.3 dex (Kobayashi & Arimoto 1999). On average, the more massive galaxies have a higher metal content than the lower mass ones. However, the small range in the final stellar masses as well as the limited number of cases presented here prevent us from considering our models as a complete subsample of typical ellipticals drawn according to some galactic mass function. Here we simply check whether our models fullfill the constraints set by the MMR and the CMR for a galaxy of ~10^{11} $M_\odot$.

For instance, we applied the Jimenez et al. (1998), photometric code to both cases Ma1 and La (inside their effective radius), and found the results in good agreement with the classic Bower et al. (1992), CMRs. By assuming an age of 12.3 Gyr (which in a standard Lambda CDM cosmology means a formation redshift of 5), we have $M_V = -20$ mag, $U - V = 1.35$ mag, $V-K = 2.94$ mag and $J-K = 0.97$ mag for model Ma1, whereas for the case La we predict $M_V = -21.3$ mag, $U - V = 1.28$ mag, $V - K = 3.17$ mag and $J - K = 1.06$ mag. It can be shown that similar results apply to all the other cases, because their star formation histories as well as their mean metallicity are roughly the same. It is known that broad-band colours poorly discriminate the details of a SF episode if this burst occurred long ago.

The models show an average $[\langle\alpha/{\rm Fe}\rangle] = 0.2$–$0.3$ as required by the observations (Worthey et al. 1992; Thomas et al. 2002; Nelan et al. 2005). In general, the predicted abundance ratios are consistent with the reported ~0.1 dex-wide observational scatter of the above-mentioned galaxies, with the exception of a few cases which will be discussed in the following sections.

On the other hand, several models (not presented here) matching the chemical properties fail to fit other observational constraints. As an example, see model Mb5, whose stellar core radius is too large by far to be taken into account in the remainder of the paper.

Model MaSN, instead, shows how a strong feedback from SN can suppress the SF process too early, as testified by the high predicted α-enhancement in the galactic core. Also in this case the galaxy is too diffuse. It can be shown that $\epsilon_{\rm SN}$ in the range 0.1–0.2 does not lead to strong variations in the results. Therefore, we adopt $\epsilon_{\rm SN} = 0.1$, in line with the calculations by Thornton et al. (1998).

In all the other cases, the dimensions of the model galaxies (i.e. their effective radii) are consistent with the values reported for bright ellipticals (e.g. Graham et al. 1996).

We stress that here we are not interested in a further fine tuning of the input parameters in order to reproduce the *typical average elliptical* as in PM04. Our aim, instead, is to understand whether it is possible to explain the observed variety of $[\langle {\rm O/Fe}\rangle]$ gradient slopes *once* all the above constraints have been satisfied. In order to do this we first examine the formation of the stellar component of a typical elliptical galaxy. Then we derive further constraints by comparing both the predicted abundance and line-strength indicex gradients with observations. Finally, we study in detail the role of several factors in shaping the $[\langle {\rm O/Fe}\rangle]$ gradients.

3.1. The outside-in formation of a typical elliptical

3.1.1. The gas-dynamical evolution

In this section we focus on the formation mechanism of a single galaxy: the time evolution of its abundance gradients will be the subject of Sect. 4.1. A clear example of a massive elliptical is given by model La (massive elliptical with the gas in intial equilibrium at 10^7 K and $\epsilon_{\rm SF} = 10$), whose chemo-dynamical evolution is shown in Figs. 1, 3–6. We will refer to this model as a reference case for characterizing the hydrodynamical behaviour of our models, as well as to derive general hints of both the development of the metallicity gradients and the SF process. We will also compare the results of model La with those of model Lb, the main difference between the two models being the initial gas distribution. Figure 1 shows the stellar and gas density profiles (upper panels) as well as the gas velocity and the temperature profiles (lower panels) at different times (see captions and labels). It can be clearly seen that at times earlier than 300 Myr the gas is still accumulating in the central regions where the density increases by several orders of magnitude, with a uniform speed across the galaxy. The temperature drops due to cooling,

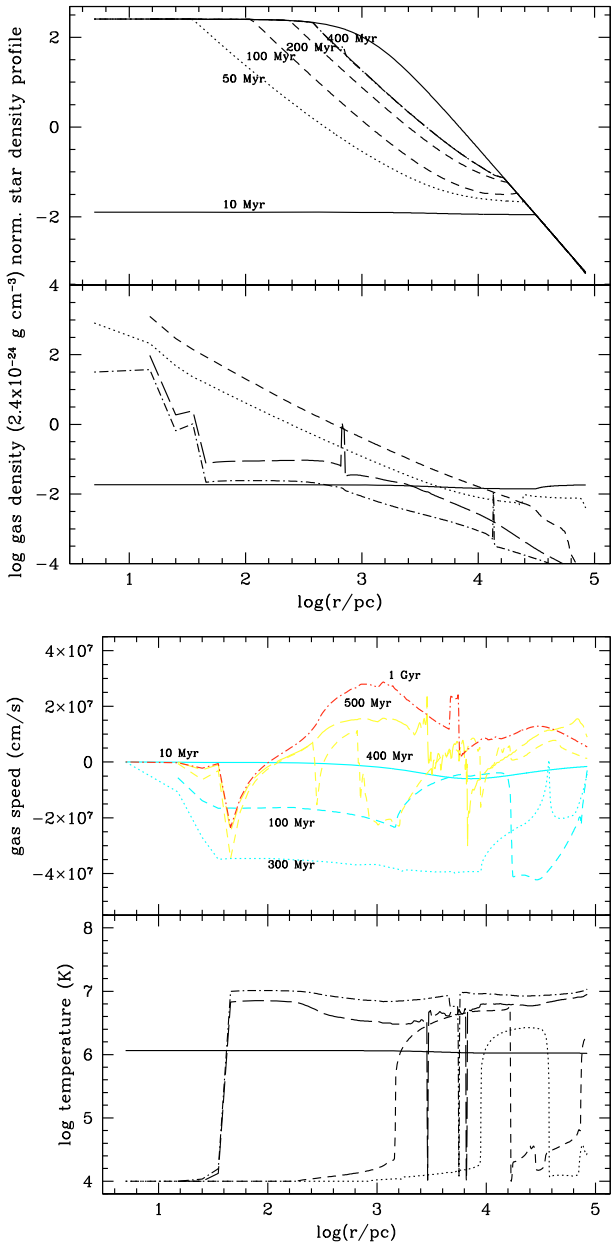

Fig. 2. Temporal evolution of density, velocity and temperature profiles for model Lb. The meaning of the curves is the same as Fig. 1.

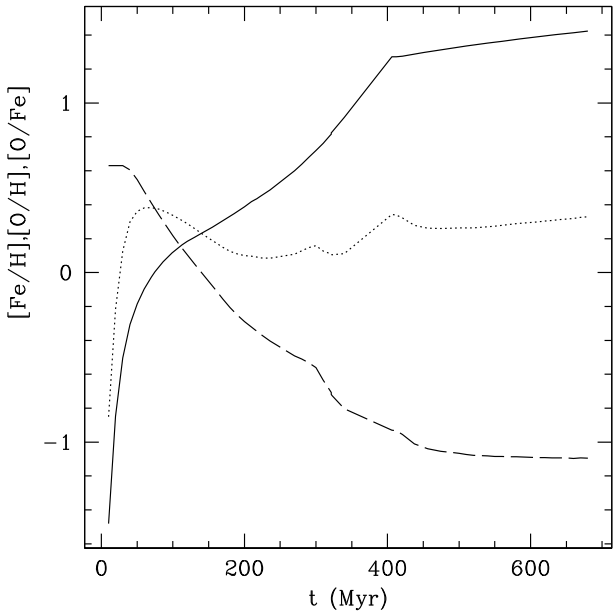

Fig. 3. Time evolution of [Fe/H] (solid), [O/H] (dotted), [O/Fe] (dashed) in the gas of model La. These abundances are values for the whole galaxy.

and the SF can proceed at a very high rate ($\sim 10^{2-3}$ $M_\odot$ yr^{-1}). In the first 100 Myr the outermost regions are built-up, whereas the galaxy is still forming stars inside its effective radius. For comparison, the thick solid line in the star density panel shows the adopted threshold (King profile). We show the evolution predicted by model Lb (similar to La, but with an initial accretion of gas) in Fig. 2. We note, that, despite the different initial conditions, the evolution of all the physically interesting quantities follows the results obtained for model La.

After 400 Myr, the gas speed becomes positive (i.e. outflowing gas) at large radii, and at 500 Myr almost the entire galaxy experiences a galactic wind. This model proves that a massive galaxy can have a galactic wind, which develops outside-in, thanks to the sole energy input from SNIa+II. The wind is supersonic for, at least, the first Gyr after $t_{\rm gw}$,which is the time of the onset of the galactic wind and depends on the model assumptions. At roughly 1.2 Gyr, the amount of gas left inside the galaxy is below 2% of the stellar mass. This gas is very hot (around 1 keV) and still flowing outside. Therefore, as anticipated by our chemical evolution studies (Pipino et al. 2002; PM04; Pipino et al. 2005), a model with a Salpeter IMF and a value for $\epsilon_{\rm SN} = 0.1$ can mantain a strong galactic wind for several Gyr, thus contributing to the ejection of the chemical elements into the surrounding medium.

The fact that the galactic wind occurs externally before internally is due to the fact that the work to extract the gas from the outskirts is less than the work to extract the gas from the center of the galaxy. Therefore, since the galactic wind occurs first in the outer regions, the star formation rate stops first in these regions, for lack of gas. In the following we will refer to *the outside-in scenario* to the fact that the SFR halts first outside then inside due to the progressive activity of the galactic wind from outside to inside.

3.1.2. Chemical abundances: from gas to stars

In Fig. 3 we show the temporal evolution of the elemental abundances in the gas for the entire galactic volume. As expected, the prompt release of O by SNII makes the [O/H] in the gas rise very quickly, whereas the Fe enrichment is delayed. As a result, the [O/Fe] ratio spans nearly two orders of magnitude, reaching the typical value set by the SNIa yields after 500 Myr. We can derive much more information from Fig. 4, where the metallicity distribution of stars as a function of [Fe/H] and [O/Fe] are shown. In these figures we plot the distribution of stars formed out of gas with a given chemical pattern (i.e. a given [Fe/H] and [O/Fe]) as contours in the [O/Fe]–[Fe/H] plane. In particular, the contours connect regions of the plane with the same mass fraction of stars. Since we consider the stars born in different points on the grid, which may have undergone different chemical evolution histories, it is useful to focus on two different regions: one limited to $R_{\rm core,*}$ (upper panel) and the other extending to $R_{\rm eff,*}$ (lower panel). It is reassuring that in both panels the overall trend of the [O/Fe] versus [Fe/H] in the stars agrees with the theoretical plot of [O/Fe] versus [Fe/H] in the gas expected from the time-delay model (Matteucci & Greggio 1986). For comparison,

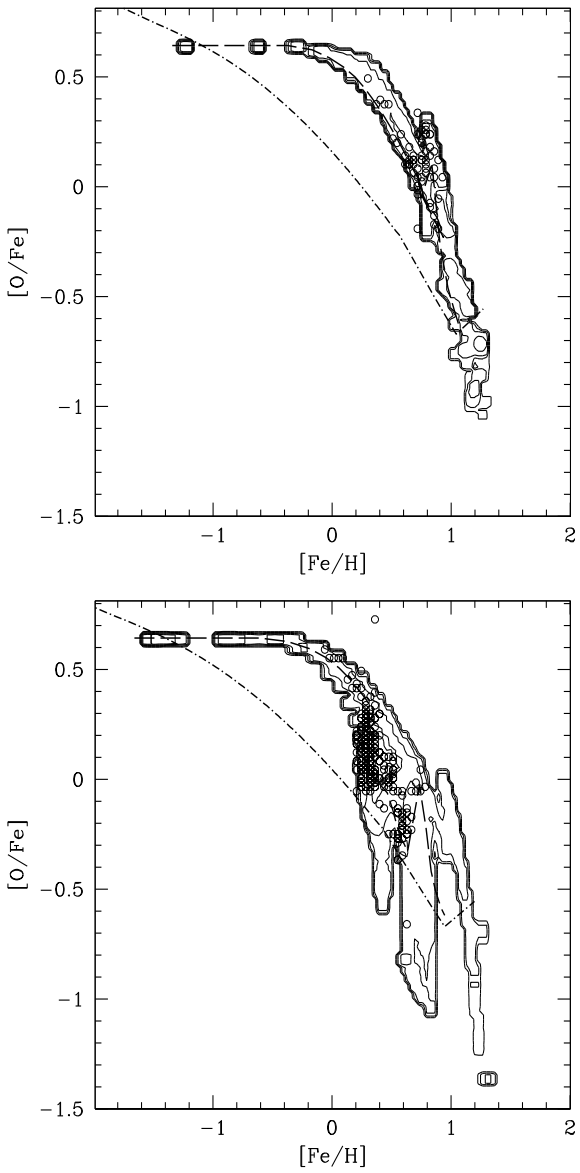

Fig. 4. Bidimensional metallicity distribution of stars as functions of [Fe/H] and [O/Fe] for the core (*upper panel*) and the effective radius regions (*lower panel*) of model La (contours). Dots: ramdomly generated stars in order to emphasize the peaks in the distributions. Dashed line: [O/Fe] vs. [Fe/H] in the gas of model La (mass-weighted values on the gridpoints of each region). Dot-dashed line: [O/Fe] vs. [Fe/H] in the gas, as predicted by the best model of PM04 for a galaxy with similar stellar mass.

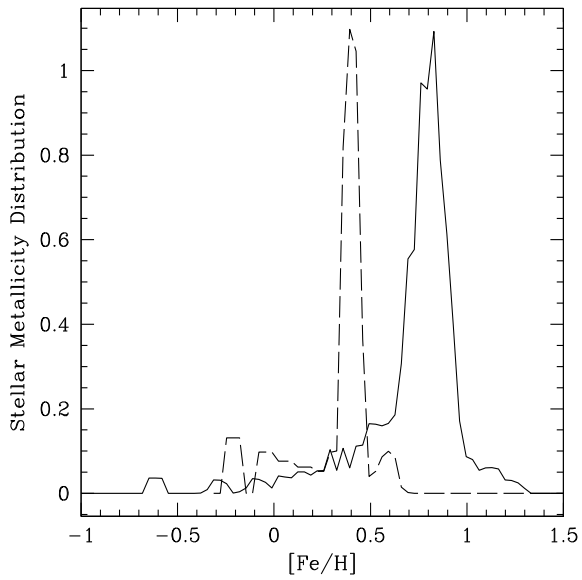

Fig. 5. The final stellar metallicity distribution as a function of [Fe/H] for model La. The values have been arbitrarily rescaled. The two peaks represent the different chemical enrichment suffered at different radii (see text). The solid line refers to the galactic core radius, whereas the dashed line is the prediction for a shell 5 kpc wide, centered at $R_{\rm eff}$.

we plot the output of PM04's best model with roughly the same stellar mass as the dot-dashed line in Fig. 4. Both the early and final stages of the evolution coincide. An obvious difference is that the *knee* in the [O/Fe] vs. [Fe/H] relation predicted by our model is much more evident than the one of PM04. The reason must be ascribed to the fact that here we adopt a fixed O/Fe ratio in the ejecta of SNII, whereas the stellar yields show that there is a small dependence on the progenitor mass (which is taken into account in detailed chemical evolution models such as the PM04 one). Moreover, as we will show in Sect. 5.1, most of the metals locked-up in the stars of the galactic core were produced outside the core. In practice, we anticipate that the inner regions suffer a metal-rich initial infall (i.e. inflowing gas has a higher [Fe/H] abundance than the gas already present and processed in the inner regions), therefore the number of stars formed at [Fe/H] ≤ -1 is very small compared to the number of stars created at very high metallicities. This rapid increase of the [Fe/H] ratio in the gas also makes the *knee* of the upper panel of Fig. 4 more evident than the one in the lower panel[2].

The above results have two implications: first, our implementation of the chemical elements in the hydrodynamical code does not produce spurious chemical effects and it has been done in the proper way. Second, it shows that a chemical evolution model gives accurate predictions of the behaviour of the mean values, even though it does not include the treatment of gas radial flows and it has a coarser spatial resolution. As expected from the preliminary analysis of PMC06, the innermost zone (Fig. 4, upper panel) exhibits less scatter. At larger radii, the distribution broadens and the asymmetry in the contours increases. This can be more clearly seen in the classical G-dwarf-like diagram of Fig. 5, where the number of stars per [Fe/H] bin only is shown. We can explain the smooth early rise in the [Fe/H]-distribution in the inner part (solid line) as the effect of the initially infalling gas, whereas the sharp truncation at high metallicities is the first direct evidence of a sudden and strong wind which stopped the star formation. The suggested outside-in formation process reflects in a more asymmetric shape of the G-dwarf diagram at larger radii (dashed line), where the galactic wind occurs earlier (i.e. closer to the peak of the star formation rate), with respect to the galactic centre. The broadening of the curves, instead, reflects the fact that the outer zone (extending to $R_{\rm eff,*}$) encloses several shells with different SF as well as gas dynamical histories.

In practice, the adopted [$\langle$Fe/H$\rangle$] and [$\langle$O/Fe$\rangle$] are either the mass or the luminosity weighted values, taken from distributions similar to the one of Fig. 5 (but on a linear scale) according to Eqs. (9) and (10). They can be compared with the SSP-equivalent values inferred from the observed spectra taken from the integrated light (see next section). These quantities tell us that models La and Lb exhibit a quite high [$\langle$Fe/H$\rangle_V$] in

[2] The physical mechanisms that produce such a metal-enhanced internal gas flows as well as their role in changing the [O/Fe] ratio in the gas, will be discussed in detail in Sect. 5.

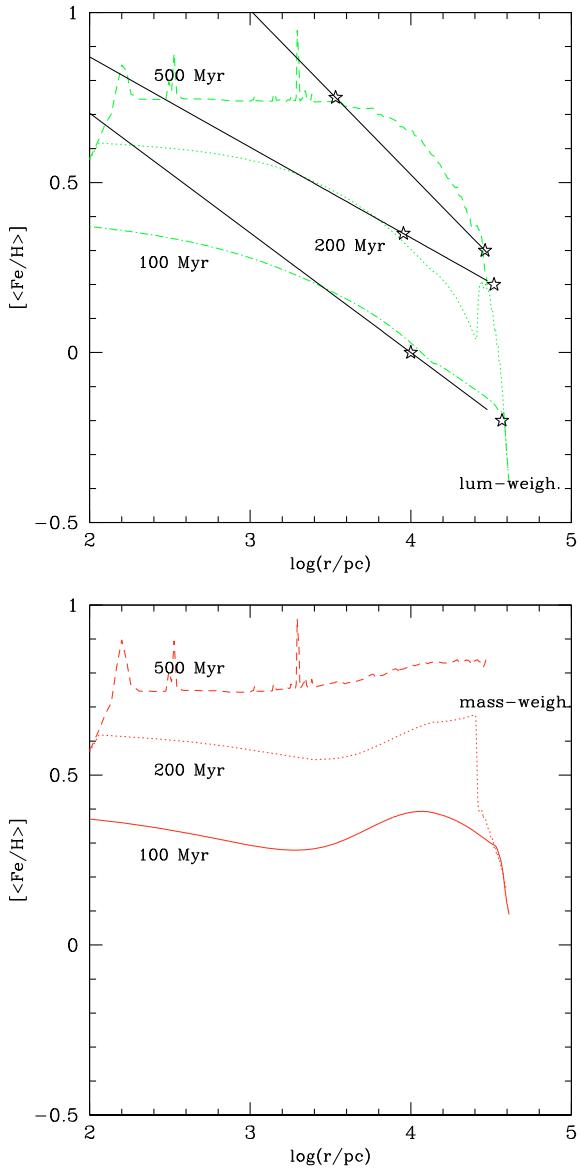

Fig. 6. Time evolution of radial metallicity gradients in stars as predicted by model La. *Upper panel*: the luminosity weighted [$\langle$Fe/H$\rangle_V$] in stars versus radius at different times (dotted-dashed: 100 Myr; dotted: 200 Myr; dashed: 500 Myr). The stars mark the luminosity-weighted values at both the core and effective radius. The solid lines represent the gradients inferred by a simple linear regression fit of the values at both the core and effective radius at each time. *Lower panel*: the mass-weighted [$\langle$Fe/H$\rangle_*$] in stars versus radius at different times (as above). The scale is the same as the upper panel. Note the differences between mass- and luminosity weighted quantities at large radii.

the stars of the galactic core, although model Lb is in slightly better agreement with the observed central values of [$\langle$Fe/H$\rangle_V$] (Carollo et al. 1993; Mehlert et al. 2003; Sanchez-Blazquez et al. 2007) than model La.

4. The formation of the abundance gradients

4.1. The temporal evolution of the gradients in the reference case

In this section we discuss the issue of radial gradients in the stellar abundance ratios. We concentrate on the *actual* gradients, namely on the ones whose properties can be measured by an observer. A snapshot of model La after 100 Myr reveals

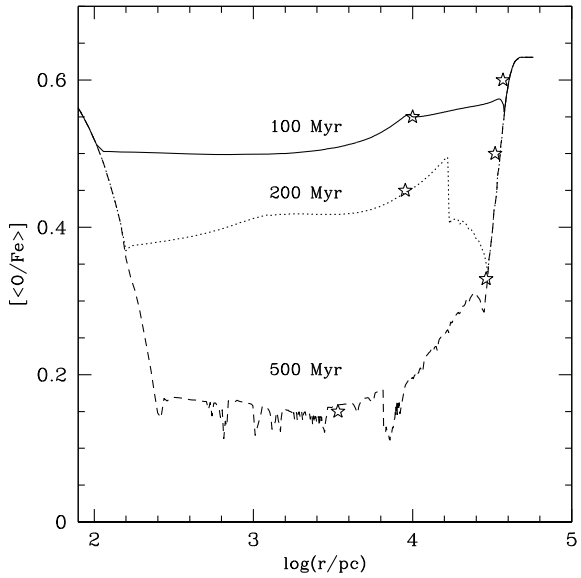

Fig. 7. Time evolution of radial [$\langle$O/Fe$\rangle$] gradient in stars predicted by model La at different times (only mass-weighted values) Solid line: 100 Myr; dotted: 200 Myr; dashed: 500 Myr.

gradients already in place with slopes $\Delta_{O/Fe} = 0.08$ (Fig. 7) and $\Delta_{Fe/H} = -0.35$ (luminosity-weighted, upper panel of Fig. 6). After the SF has been completed, we have $\Delta_{O/Fe} = 0.19$ and $\Delta_{Fe/H} = -0.5$, respectively. Both values are consistent with the predictions by PM04. In the same time interval, $R_{core,*}$ and $R_{eff,*}$ decrease by a factor of 3 and 1.5, respectively. The changes in these quantities are more evident if we look at other models such as Ma1, where the final $R_{core,*}$ and $R_{eff,*}$ are smaller by a factor of 5 and 2 than the *initial* ones. In this case, however, the slope in the [$\langle$O/Fe$\rangle$] changes more smoothly from –0.024 to 0.02, whereas the steepening in the Fe gradient (from 0.48 to –0.13) is more dramatic.

Thus both models Ma1 and La experience an outside-in formation process that creates the abundance gradients within the observed range, although with different slopes. The galactic winds play a role in the gradients build-up. The temporal evolution of the gradients for model La can be visualized in Fig. 6, where the mass-weighted values for the [$\langle$Fe/H$\rangle$] are also displayed in the bottom panel. As expected from the analysis of PMC06, mass-weighted values might differ from luminosity-weighted quantities with increasing galactocentric radii, because of the well-know strong metallicity dependence of light in the optical bands. In this particular case, we predict a quite flat gradient, when the mass-weighted values are taken into account. This happens because at large radii there is a significant number of very metal-rich stars, even though the peak of the stellar metallicity distribution (see Fig. 5) occurs at a lower [Fe/H] than in the core. There are many other effects that generate this apparent dichotomy between peak values and averages. First, the stellar metallicity distributions are generally asymmetric, thus the mathematical average does not coincide with the distribution's *mode* (i.e. the peak value, see PMC06). Secondly, the integral in Eq. (9) is performed by taking into account a linear sampling of star mass in Fe/H bins (instead of [Fe/H]). Thus [$\langle$Fe/H$\rangle$] is always higher than $\langle$[Fe/H]$\rangle$ (see Gibson 1997). Therefore taking the observed (i.e. luminosity-weighted) gradients at their face value might not necessarily reflect the actual galaxy formation process. Moreover all these subtle differences in the choice of a SSP-equivalent value (either [$\langle$Fe/H$\rangle$] or $\langle$[Fe/H]$\rangle$ or simply [Fe/H]$_{peak}$) might lead to different final values for our gradients.

To guide the eye, in the upper panel of Fig. 6 the solid lines represent a linear regression fit of the mean (luminosity weighted) abundances, at each time, at the core and at the effective radius. If an observer measures the abundance at both $R_{\rm core,*}$ and $R_{\rm eff,*}$ and then tries to infer a metallicity gradient by a linear regression (i.e. a straight line of slope $\Delta_{\rm Fe/H}$), the difference between those findings and the actual behaviour of [⟨Fe/H⟩] versus the radius can be large.

By means of these models we have shown that a 10% SN efficiency, as adopted in purely chemical models (PM04; PMC06; Martinelli et al. 1998), is supported also by hydrodynamical models. Also, we note that models with 100% SN efficiency (e.g. MaSN) experience the galactic wind too early in their evolution, thus implying that their chemical properties are at variance with observations.

4.2. Gradients in Fe/H and total metallicity

We find a radially decreasing luminosity-weighted Fe abundance in all our models: $\Delta_{\rm Fe/H}$ spans the range –0.5 −–0.2 dex per decade in radius, with a mean value of –0.25, in good agreement with the analysis of Kobayashi & Arimoto (1999). Once transformed into observables by means of 12 Gyr old TMB03 SSPs, the predicted gradient slopes are $\mathrm{d\,Mg_2/\log(R_{core,*}/R_{eff,*})} \sim -0.06$ mag per decade in radius, again in agreement with the typical mean values measured for ellipticals by several authors and confirming the PM04 best model predictions. We notice that for models such as Mb3 and Ma2, we obtain $\mathrm{d\,Mg_2/\log(R_{core,*}/R_{eff,*})} \sim -0.1$ mag per decade in radius, possibly matching a few objects in the sample of Ogando et al. (2005, see also Baes et al. 2007). This conclusion is strenghtened by the fact that the *total* metallicy gradients also are similar between the models, their slopes typically being $\mathrm{d([\langle Z/H\rangle_V])/\log(R_{core,*}/R_{eff,*})} \sim -0.2 - -0.3$ dex per decade in radius, in agreement with the average value of the Annibali et al. (2007) sample, with the exception of model Ma2 (an average elliptical with the gas initially in equilibrium at 10^4 K – as well as $\epsilon_{\rm SF} = 10$) whose slope of $\mathrm{d([\langle Z/H\rangle_V])/\log(R_{core,*}/R_{eff,*})} = -0.42$ dex per decade in radius is close to the largest gradients observed in the galaxies in the sample of Ogando et al. (2005).

The build-up of such gradients can be explained by the non-negligible role of the galactic wind, which occurs later in the central regions, thus allowing a larger chemical enrichment with respect to the galactic outskirts. The predicted gradient slopes are independent of the choice of the intial setup given by either case *a* or *b*. We are conscious, however, that we relaxed the PM04 hypothesis of non-interacting shells; therefore, in the rest of the paper we will also highlight the role of the metal flows toward the center.

4.3. Gradients in O/Fe

Mehlert et al. (2003), Annibali et al. (2007), and Sanchez-Blazquez et al. (2007) have shown a complex observational situation relative to abundance gradients, especially the gradients of the [α/Fe] ratio. A successful galactic model should be able to reproduce the [α/Fe] radial stellar gradient, either if flat or negative, while keeping fixed all the other properties (including the [⟨Fe/H⟩$_V$] gradient). This is nearly impossible with standard chemical evolution codes, unless one uses extreme assumptions which may worsen the fit of all the other observables.

The hydro-code presented in this paper helps us in tackling this issue. From the entries in Table 2, we notice that all the objects that present reasonable values for their chemical properties, including the [⟨Fe/H⟩$_V$] gradient, show a variety of gradients in the [α/Fe] ratio, either positive or negative, and one model shows no gradient at all (Mb2, namely an average elliptical with the gas initially diffuse and cold – 10^4 K – as well as $\epsilon_{\rm SF} = 10$).

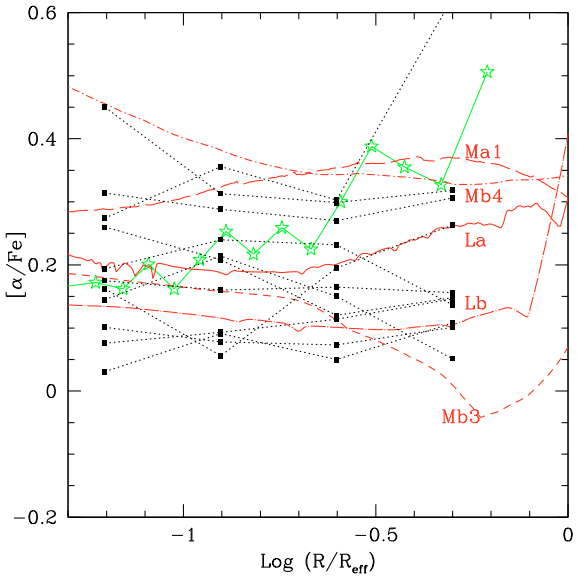

Fig. 8. [⟨O/Fe⟩] gradients predicted by several models compared to a subsample of Annibali et al. (2007)'s data (full squares connected by dotted lines) and the data for NGC 4697 (stars).

A comparison between some of our models and data drawn from Annibali et al. (2007) (namely a subsample of only massive ellipticals with homogeneously measured gradients out to $0.5R_{\rm eff}$) is made in Fig. 8. Also the data for NGC 4697 are reported. The models predict a relationship between the abundance ratios and the radius which is not linear. This further complicates the comparison with observations and will be the subject of a future paper. As an example the Annibali et al. (2007) sample is limited to $\sim R_{\rm eff,*}/2$; therefore, it is not surprising that their mean slopes are smaller than expected if one takes into account the whole region $R_{\rm core,*} \leq R \leq R_{\rm eff,*}$. However the agreement with our model is very good, when considering the same galactic regions, see Fig. 8

As expected from this comparison, the predicted values for $\Delta_{\rm O/Fe}$ span a range from –0.2 to +0.3, which is similar to the observed one (e.g. Mehlert et al. 2003), with an average gradient slope of –0.002 dex per decade in radius.

Remarkably, this occurs in spite of the fact that the galaxy formation process always proceeds outside-in.

No correlations between $\Delta_{\rm O/Fe}$ and other galactic properties are found, as expected from observations. The galaxies showing the steepest (both positive and negative) [⟨O/Fe⟩] gradient slope, also have a quite strong radial decrease in the [⟨Fe/H⟩$_V$] ratio, although a quantitative confirmation needs a sample statistically richer than ours. A correlation in this sense seems to emerge in the Annibali et al. (2007) data (Annibali, private communication).

In the case of model Ma2, we predict $\Delta_{\rm O/Fe} = -0.21$, but it has almost the same final stellar mass as both models La and Lb, only being more compact, and it shows average abundance ratios in stars matching the typical mean values observed for massive ellipticals. On the other hand, model Mb4 (as is Ma1, the only difference is that the gas is diffuse at the beginning) has a gradient of $\Delta_{\rm O/Fe} = -0.08$ and model Mb1 predicts $\Delta_{\rm O/Fe} = 0.11$. All these models stop the SF at $R \geq R_{\rm eff,*}$ earlier than in the core.

5. Possible explanations for the observed variety of [⟨O/Fe⟩] radial gradient slopes

We have analysed the possible causes for the variety of the predicted gradients in the abundance ratios: metal-enhanced radial flows and variable timescale of SF with radius. Here we disentangle their different roles by studying the effects of the gas flows in determining the central values (i.e. the $[\langle O/Fe\rangle_{core,*}]$), whereas the variation of the SF timescale along the radius will be mainly linked to the gradient slope. We stress that the results we present here and their interpretation is valid for the particular initial conditions that we explored. Therefore, the intial set-up of the simulations is a sufficient condition for such a variety of gradients to be created.

5.1. Radial gas flows

In order to understand the differences - both observed and predicted – in the [α/Fe] gradients among ellipticals, we first study the gas composition in a sphere of radius $R_{core,*}$ at each timestep. In this way we can obtain insights into the role of the gas flows in the determination of $[\langle O/Fe\rangle_{core,*}]$.

Almost all the models predict that, after the first 100 Myr, a substantial fraction (i.e. 80–90%) of the metals present in the gas inside $R_{core,*}$ has an external (i.e. $R_{core,*} < R < R_{tidal,*}$) origin. This means that a non-negligible contribution to the gradients is from the gas flows, as shown by the negative velocity field for $t < t_{gw}$ in Figs. 1 and 2, and this is also expected in dissipative models such as the Larson (1974) and the Carlberg (1984) ones. This effect cannot be seen in standard chemical evolution models with non-interacting shells, where, at a fixed mass, the predicted $\Delta_{Fe/H}$ is always smaller than in the models presented in this paper (e.g. see Table 5 of PM04).

In order to quantify the effects of the convolution of the SF with the gas flows, we use Eq. (9) to define, for a given chemical element, the mass-weighted ratio $\mathcal{R}$ between the mass of this element produced in the galactic core and locked-up in stars to the amount produced in a more external region (and subsequently locked-up in stars inhabiting the core). In particular, for O we define the quantity $\mathcal{R}_O$ as:

$$\mathcal{R}_O = \frac{1}{S_{f,core}} \int_0^{S_{f,core}} (O_{out}/O)(S)\, dS, \qquad (11)$$

where, at variance with Eq. (9), we now consider the distribution of stars as a function of the ratio (O_{out}/O) and extract its average. In this case O_{out} is the mass of O produced in the external (i.e. outside $\sim 3 \times R_{core,*}$) part of the galaxies, sunk in the galactic centre because of the radial inflows and eventually locked-up in stars inhabiting the core[3]. On the other hand, O is the *actual* mass of oxygen out of which stars form inside a sphere of radius $R = R_{core,*}$. A high efficiency of the radial flows in transferring O from the external regions of the galaxy will correspond to high values of the ratio $\mathcal{R}_O$. On the other hand, $\mathcal{R}_O = 0$ means that all the stars formed in the core incorporate only the O produced by the previous generations that populated the core. We also evaluate the same ratio in the case of Fe, namely $\mathcal{R}_{Fe}$. Both the $\mathcal{R}_O$ and the $\mathcal{R}_{Fe}$ time evolutions for four selected models are shown in Table 3. These quantities give an estimate of the contribution of the metal rich radial flows to the build-up of the gradients. The last row of Table 3 shows the quantity $[\langle O/Fe\rangle_{*,core,noflux}]$, namely the expected central value of the $[\langle O/Fe\rangle_*]$ in the hypothetical case in which the metals produced outside $\sim 3 \times R_{core,*}$ do not flow into the core (to be compared to the entries of Table 2, 6th column).

Remarkably 3/4 of the models have $[\langle O/Fe\rangle_{*,core,noflux}] = 0.3$.

In model Ma1, the mild positive $\Delta_{O/Fe}$ is not enhanced by the metal rich gas produced in the outskirts and flowing toward the center because $\mathcal{R}_{Fe}$ and $\mathcal{R}_O$ evolve in parallel because they are dominated by the external production of metals in the same way (see Table 3).

In other cases, such as the model Mb3 (average elliptical with the gas initially diffuse and hot – 10^6 K – as well as $\epsilon_{SF} = 10$), instead, we have $\mathcal{R}_{Fe} > \mathcal{R}_O$. This model starts from a uniform gas distribution, then most of the gas out of which the stars form must first have sunk into the centre. As a consequence, the star formation rate peaks later than model Ma1. On the other hand, the outermost regions stop their star formation process, and thus O production, quite soon; therefore, most of the stars in the central regions preferentially lock the Fe which is coming from the SNIa exploding in the outskirts, rather than O. This explains the slightly low central [⟨O/Fe⟩], despite the high SF parameter ($\epsilon_{SF} = 10$); $\Delta_{O/Fe}$ is ∼0.18 at 100 Myr, ∼0 at 240 Myr and becomes negative soon after.

As anticipated above, due to the very high star formation rate (with respect to the gas inflow rate) in model Lb we have the lowest $\mathcal{R}_{Fe}$ and $\mathcal{R}_O$, therefore the gradient could reflect the real outside-in formation in a manner that resembles the multi-zone chemical evolution models with non-interacting shells. Nevertheless, also in this case, we have $\mathcal{R}_{Fe} > \mathcal{R}_O$, which is the outcome of a differential inflow, as explained above for model Mb3.

In summary, radial flows may lower the core value of [⟨O/Fe⟩] (that we consider as the zero point of the gradient in [α/Fe]) relative to the case with no radial flows. The reason for that is that α-depleted material flows from the outermost into the innermost regions. Therefore, the variety of gradients (in particular positive, null or negative) depends on the efficiency of the α-depleted gas to flow from the outside to the inside during the time of active star formation. In other words, it depends on the velocity of the inflowing gas. Clearly a larger or smaller parameter of SF can have a strong influence on this process. In order to help the visualization of such a complex process, we show Fig. 9 where the solid line at the top represents a hypothetical *pure outside-in model* with non-interacting shells and $[\langle O/Fe\rangle_{*,core,noflux}] = 0.3$. The gradient slope is chosen to be 0.15 dex per decade in radius. In this case the [⟨O/Fe⟩] gradient is set by the occurrence of the galactic wind, which happens earlier in the outermost regions. Such a model is not real. It helps in visualising the simplest scenario – which is quite a common assumption in the literature involving multi-zone chemical evolution modelling – and the differences introduced by taking into account radial flows and the local variation in the *input* star formation timescale. None of the models correspond to this ideal case, therefore we cannot compare it with any of our predicted curves.

In order to take into account the role of the gas flows we then correct the predicted gradient (solid line in the middle), thus obtaining something similar to the predictions by models La (dashed line) and Lb. This mechanism helps also in explaining the value for $[\langle O/Fe\rangle_{*,core}]$ predicted by other models, such as Mb3 (dotted line).

[3] We only subtract from the metal budget, a posteriori, those elements not produced in situ and followed in their evolution by means of a suitable tracer.

Table 3. Contribution to the core abundances by metals produced in more external regions.

t (Gyr)	$\mathcal{R}_O$				$\mathcal{R}_{Fe}$			
	Ma1	Mb4	Mb3	Lb	Ma1	Mb4	Mb3	Lb
0.05	0.49	0.66	0.82	0.23	0.49	0.66	0.82	0.21
0.07	0.70	0.75	0.84	0.45	0.69	0.74	0.84	0.42
0.10	0.81	0.82	0.85	0.58	0.80	0.82	0.86	0.56
0.15	0.86	0.79	0.78	0.67	0.85	0.82	0.83	0.67
0.20	0.88	0.76	0.72	0.64	0.87	0.82	0.80	0.73
0.30	0.89	0.76	0.64	0.57	0.89	0.81	0.74	0.72
final	0.89	0.76	0.64	0.57	0.89	0.81	0.74	0.72
$[\langle O/Fe\rangle_{*,core,noflux}]$	0.27	0.51	0.33	0.30				

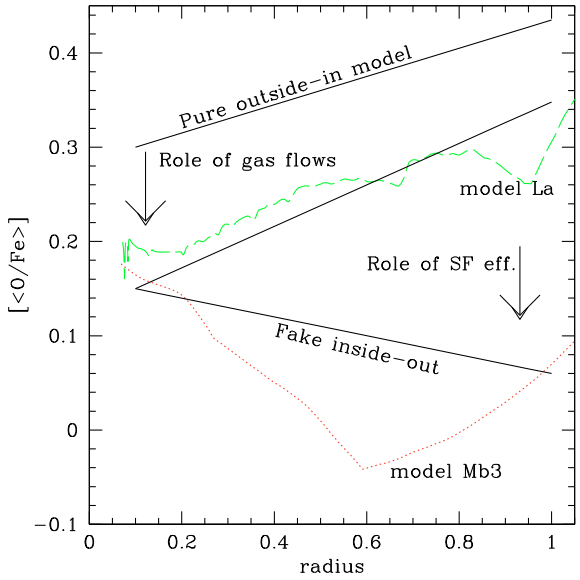

Fig. 9. The relative contribution of the gas flows strength and the star formation parameter ν to the creation of the final gradient for two particular cases: model La's predicted gradient (positive slope, *dashed line*); model Mb3's predicted gradient (negative slope, *dotted line*). *Pure outside-in model:* hypothetical model with an outside-in formation, $[\langle O/Fe\rangle_{*,core,noflux}] = 0.3$ (no gas flows) and ν constant with radius; *fake inside-out model:* hypothetical model with a strong variation of the star formation timescale with radius. The abscissa is expressed in units of the effective radius.

5.2. The role of the star formation timescale at different radii

Let us examine now the effect of varying the SF timescale. The analysis of the mass-weighted abundance ratio in the inner zone is not enough to explain the gradients. We have studied only the build-up of the zero-point value, taken as the quantity $[\langle O/Fe\rangle_{*,core}]$. Even in the simplistic assumption in which the gradient can be well represented by a straight line we need another quantity in order to fix the slope steepness. We chose to study the radial variation of t_{cool} and t_{ff}, because another important difference with respect to PM04 and PMC06 is that here $\nu = \frac{\epsilon_{SF}}{\max(t_{cool}, t_{ff})} \neq$ const.

We find that ν(core) $\sim 2 - 3 \times \nu(R_{eff})$ in a model such as Lb, which closely follows the PM04 best model. On the other hand, models with either a zero or a negative $\Delta_{O/Fe}$ have ν(core) $\sim$ 5–$10 \times \nu(R_{eff})$ for most of their evolution, thus favouring a higher [O/Fe] ratio in the stars belonging to the inner regions. Other test cases, not presented here, show that if we run models with even higher values for the star formation parameter (i.e. $\epsilon_{SF} \geq 20$), the strong feedback by SNe halts the gas flow; therefore the supply of baryons for SF in the galactic center is strongly reduced and the outcome is a too diffuse galaxy. A similar result can be obtained by increasing ϵ_{SN}, as shown by model MaSN.

The radial variation of ν means that the effect of the outside-in formation could be balanced by the interplay between local differences in the SF timescale and differential gas flows. Therefore the combined effect of gas flows plus a strong variation in the star formation timescale along the radius make the *hypothetical outside-in model* gradient change slope (line labelled as *fake inside-out model* in Fig. 9), thus matching the average trend predicted by model Mb3 (dotted line).

In general, $\Delta_{O/Fe}$ seems to fluctuate around a null value and to be a result of the interplay of many hydrodynamical factors which render it more sensitive to the initial conditions of the gas rather than an indicator of the chemical enrichment process. Possible connections between the above-mentioned trends and the other galactic properties will be investigated in a future paper.

The gradients in $[\langle Fe/H\rangle_V]$ and $[\langle Z/H\rangle_V]$ may be affected by the particular formation history of a model only in their zero point, whereas their slopes are shaped by the strong role of the gas flows (both the final values of $\mathcal{R}_{Fe}$ and $\mathcal{R}_O$ are always larger than of 50%) and by the fact that the SF always proceeds outside-in.

Another important point is that the differences among the values of $\Delta_{O/Fe}$ in the models presented in this paper are typically around a factor of 2 (if they are not presented in logarithmic units), values which are probably comparable to all the uncertainties involved in the measurements of the gradients as well as uncertainties related to the transformation from indices to abundances of such quantities (see PMC06). This calls for newer, larger as well as homogeneous samples of gradients observed in ellipticals and extended to one effective radius. Only then, it will be possible to discriminate between the particular models presented in this work.

6. Conclusions

In this paper we have studied the formation and evolution of ellipticals by means of hydrodynamic models in which we implement detailed prescriptions for the chemical evolution of H, He, O and Fe, thus presenting a detailed treatment of both the chemical and the gas-dynamical evolution of elliptical galaxies. Within this framework we are able to relax the assumption of non-interacting shells which hampers many chemical evolution codes in the modelling of the gas flows, thus allowing us to perform a detailed study of the build-up of the metallicity gradients in stars. We suggest an outside-in formation for the majority of ellipticals in the context of the SN-driven wind scenario, thus confirming previous results of chemical evolution models, but

we also show the necessity of taking into account in detail gas inflows/outflows.

Here we summarise our main results.

- We find $\Delta_{Fe/H}$ in the range –0.5–-0.2 dex per decade in radius and $\Delta_{Z/H} \sim -0.3$ dex per decade in radius, in agreement with observations (e.g. Kobayashi & Arimoto 1999).
- These gradients in the abundances, once transformed into predictions of the line-strength indices, lead to $dMg_2/\log(R_{core,*}/R_{eff,*}) \sim -0.06$ mag per decade in radius, again in agreement with the typical mean values measured for ellipticals and confirming the PM04 best model predictions. We also find that some models predict a steeper gradient, and this seems to be in agreement with the observed gradients of a few massive objects in the Ogando et al. (2005) sample.
- The build-up of the gradients is very fast and we predict negligible evolution after the first 0.5–1 Gyr.
- Most of the galactic models predict that stars form outside-in, as suggested by PMC06.
- We also find the *actual* (i.e. mass-averaged) metallicity gradients can be flatter than the luminosity-weighted ones (i.e. the observed ones).
- The main novelty of this work is that we address the issue of the observed scatter in the radial gradient of the mean stellar [α/Fe] ratio and its apparent lack of correlation with all the other observables. By analysing typical massive ellipticals, we find that all the models that predict chemical properties, including the [$\langle$Fe/H$\rangle_V$] and the global metallicity gradient, within the observed ranges, show a variety of gradients in the [α/Fe] ratio, either positive, negative or null.
- We explain this finding by the fact that the suggested outside-in mechanism for the formation of the ellipticals is not the only process responsible for the formation of abundance gradients. In particular, other processes should be considered such as the interplay between local differences in the SF timescale and gas flows. In particular, our models suggest the gradient in the [α/Fe] ratio to be be related to the interplay between the velocity of the α-enhanced radial flows, moving from the outer to the inner galactic regions, and the intensity and therefore duration of the SF formation process at any radius. In other words, if the flow velocity is fast relative to the star formation, the stars still forming at inner radii have time to form out of α-enhanced gas coming from the outermost regions, thus flattening and even reversing the sign of the [α/Fe] gradient.
- In particular, we have shown that we do not need the merger events invoked in order to have a shallow [$\langle\alpha$/Fe$\rangle$] gradient.
- Moreover, the predicted age gradients are very small, being typically a few Myrs per decade in radius, in agreement with Sanchez-Blazquez et al. (2007). This means that the estimate of the *relative* duration of the SF process between two different galactic regions by measuring the [$\langle$O/Fe$\rangle$] is not a robust method. In other cases in which, instead, the age gradients are stronger we expect much more evident radial variations in the [$\langle$O/Fe$\rangle$], such as those outlined in PMC06.
- According to our fiducial cases, up to 90% of the metals locked in stars in the galactic center could have been synthesized at larger radii.

The new class of models presented here make several new predictions about both the shape and the *fast* evolution of the metallicity gradients that are left unconstrained by the lack of observations. What makes galaxies start from quasi-monolithic conditions is still to be understood. The quest for an explanation of such behaviours will be a challenging field of research if future observation campaigns will confirm the steep positive $\Delta_{O/Fe}$ found in, e.g., NGC 4697 (see Fig. 8), and thus, further validate a particular type of models. These observables will be the test of our suggested galaxy formation scenario to be provided by future observations.

Acknowledgements. We acknowledge useful discussions with F. Annibali, L. Ciotti. Then we warmly thank F. Calura, C. Chiappini, S. Recchi and P. Sanchez-Blazquez for a careful reading of the paper and many enlightening comments. The work was supported by the Italian Ministry for the University and the Research (MIUR) under COFIN03 prot. 2003028039.

References

Annibali, F., Bressan, A., Rampazzo, R., Zeilinger, W. W., & Danese, L. 2007, A&A, 463, 455
Arimoto, N., & Yoshii, Y. 1987, A&A, 173, 23
Asplund, M., Grevesse, N., & Sauval, A. J. 2005, ASPC, 336, 25
Baes, M., Silchenko, O. K., Moiseev, A. V., & Manakova, E. A. 2007, A&A, 497, 991
Bedogni, R., & D'Ercole, A. 1986, A&A, 157, 101
Bower, R. G., Lucey, J. R., & Ellis, R. S. 1992, MNRAS, 254, 589
Carlberg, R. G., ApJ, 286, 403
Carollo, C. M., Danziger, I. J., & Buson, L. 1993, MNRAS, 265, 553
Ciotti, L., D'Ercole, A., Pellegrini, S., & Renzini, A. 1991, ApJ, 376, 380
Davies, R. L., Sadler, E. M., & Peletier, R. F. 1993, MNRAS, 262, 650
Forbes, D. A., Sanchez-Blazquez, P., & Proctor, R. 2005, MNRAS, 361, 6
Friaca, A. C. S., & Terlevich, R. J. 1998, MNRAS, 298, 399
Gibson, B. K. 1996, MNRAS, 278, 829
Gonzalez, J. J., & Gorgas, J. 1996, in Fresh Views of Elliptical Galaxies, ed. A. Buzzoni, A. Renzini, & A. Serrano, ASP Conf. Ser., 86, 225
Graham, A., Lauer, T. R., Colless, M., & Postman, M. 1996, ApJ, 465, 534
Greggio, L. 2005, A&A, 441, 1055
Harris, W. E., & Harris, G. L. H. 2002, AJ, 123, 3108
Iwamoto, K., Brachwitz, F., Nomoto, K., et al. 1999, ApJS, 125, 439
Jimenez, R., Padoan, P., Matteucci, F., & Heavens, A. F. 1998, MNRAS, 299, 123
Kobayashi, C. 2004, MNRAS, 347, 740
Kobayashi, C., & Arimoto, N. 1999, ApJ, 527, 573
Larson, R. B. 1974, MNRAS, 166, 585
Lee, H.-C., & Worthey, G. 2005, ApJS, 160, 176
Martinelli, A., Matteucci, F., & Colafrancesco, S. 1998, MNRAS, 298, 42
Matteucci, F. 1992, ApJ, 397, 32
Matteucci, F. 1994, A&A, 288, 57
Matteucci, F., & Greggio, L. 1986, A&A, 154, 279
Matteucci, F., Panagia, N., Pipino, A., et al. 2006, MNRAS, 372, 265
Matteucci, F., & Recchi, S. 2001, ApJ, 558, 351
McCarthy, I. G., Bower, R. G., & Balogh, M. L. 2006 [arXiv:astro-ph/0609314]
Mehlert, D., Thomas, D., Saglia, R. P., Bender, R., & Wegner, G. 2003, A&A, 407, 423
Mendez, R. H., Thomas, D., Saglia, R. P., et al. 2005, ApJ, 627, 767
Nelan, J. E., Smith, R. J., Hudson, M. J., et al. 2005, ApJ, 632, 137
Ogando, R. L. C., Maia, M. A. G., Chiappini, C., et al. 2005 ApJ, 632, 61
Padovani, P., & Matteucci, F. 1993, ApJ, 416, 26
Pagel, B. E. J., & Patchett, B. E. 1975, MNRAS, 172, 13
Peletier, R. F., Davies, R. L., Illingworth, G. D., Davis, L. E., & Cawson, M. 1990, AJ, 100, 1091
Pipino, A., & Matteucci, F. 2004, MNRAS, 347, 968 (PM04)
Pipino, A., Matteucci, F., Borgani, S., & Biviano, A. 2002, NewA, 7, 227
Pipino, A., Matteucci, F., & Chiappini, C. 2006, ApJ, 638, 739 (PMC06)
Proctor, R. N., Forbes, D. A., Forestell, A, & Gebhardt, K. 2005, MNRAS, 362, 857
Salpeter, E. E. 1955, ApJ, 121, 161
Sanchez-Blazquez, P., Forbes, D. A., Strader, J., et al. 2007, [arXiv:astro-ph/0702572]
Serra, P., & Trager, S. 2007, MNRAS, 374, 769
Silich, S. A., & Tenorio-Tagle, G. 1998, MNRAS, 299, 249
Sutherland, R. S., & Dopita, M. A. 1993, ApJS, 88, 253
Thomas, D., Maraston, C., & Bender, R. 2003, MNRAS, 339, 897
Thornton, K., Gaudlitz, M., Janka, H.-T., & Steinmetz, M. 1998, ApJ, 500, 95
Trager, S. C., Faber, S. M., Worthey, G., & Gonzalez, J. J., 2000a, AJ, 119, 1654
Yoshii, Y., & Arimoto, N. 1987, A&A, 188, 13
Worthey, G., Faber, S. M., & Gonzalez, J. J. 1992, ApJ, 398, 69